Journal of Materials Chemistry A

Accepted Manuscript

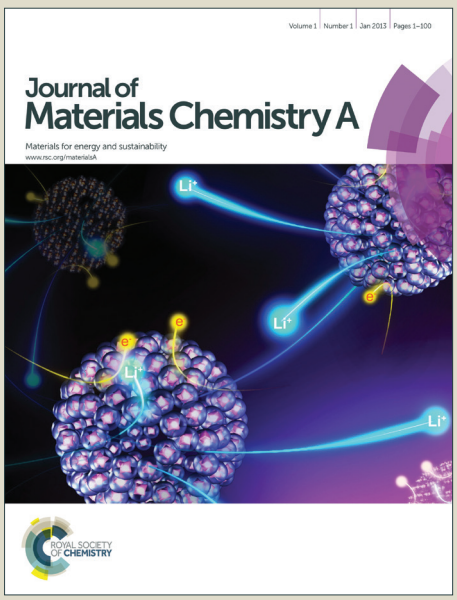

ROYAL SOCIETY OF CHEMISTRY

www.rsc.org/materialsA

Journal of Materials Chemistry C
Journal of Materials Chemistry A
Dynamic Article Links ►

Cite this: DOI: 10.1039/c0xx00000x

www.rsc.org/xxxxxx

Full Papers

Highly Activated K-Doped Iron Carbide Nanocatalysts Designed by Computational Simulation for Fischer-Tropsch Synthesis

Ji Chan Park,[a] Sang Chul Yeo,[b] Dong Hyun Chun,[a] Jung Tae Lim,[c] Jung-Il Yang,[a] Ho-Tae Lee,[a] Sungjun Hong,[a] Hyuck Mo Lee,[b] Chul Sung Kim,[c] and Heon Jung*[a]

Received (in XXX, XXX) Xth XXXXXXXXX 20XX, Accepted Xth XXXXXXXXX 20XX
DOI: 10.1039/b000000x

Although the reaction results of numerous iron-based Fischer-Tropsch synthesis catalysts containing various promoters have been reported, the research on their theoretical foundation is still insufficient. In the present work, highly activated K-doped χ-Fe_5C_2/charcoal nanocatalysts were designed using calculations based on density functional theory (DFT), and then prepared using a melt-infiltration process and a subsequent incipient-wetness method of K precursors. The catalyst at K/Fe=0.075 in an atomic ratio that bear small iron carbide nanoparticles of ~18 nm showed the highest activity (1.54×10^{-4} $mol_{CO}\bullet g_{Fe}^{-1}\bullet s^{-1}$) and the best hydrocarbon yield (1.41×10^{-3} $g_{HC}\bullet g_{Fe}^{-1}\bullet s^{-1}$), as well as good selectivity for gasoline-range (C_5-C_{12}) hydrocarbon products in the high-temperature Fischer-Tropsch reaction.

1. Introduction

Fischer-Tropsch synthesis (FTS) is known as an effective method for producing long straight-chain hydrocarbons, by a surface polymerization reaction, from a mixture of CO and H_2 gasses.[1-4] In particular, high-temperature FTS reaction, which is normally conducted at temperatures of 300-350°C, has been a key technology for producing automotive gasoline components and lower olefins from fossil resources (e.g., natural gas, biomass, or coal).[5-7]

In the preparation of the catalyst, the choice of porous support materials is crucial to guarantee the uniform dispersion of active metal particles and to protect from severe agglomeration of the catalyst particles. Until now, various Fe-supported catalysts using γ-Al_2O_3, SiO_2, and MgO have been applied to the FTS reaction.[8-10] However, when these metal-oxide supports were used, a strong metal-support interaction was also generated, leading to difficulties in reduction and activation to catalytically active phase(s). For high-temperature reactions, porous carbon materials such as activated charcoal/carbon appears to be good candidates for catalyst support due to their high chemical stability, good thermal conductivity, and weak metal-carbon interaction.[11-15] Recently, Galvis et al. showed high activity using a Fe-on-carbon-nanofiber (CNF) catalyst as well as good selectivity for lower olefins in high temperature FTS.[16-17]

Because iron-oxides (Fe_2O_3, Fe_3O_4), metallic iron, and iron carbides usually coexist during FTS, the exact determination of the real active phases is very difficult. Although the identity of the active phases remains controversial, the monoclinic Hägg-carbide (χ-Fe_5C_2) has been considered one of the most important active species among several iron, iron oxide, and iron carbide phases (e.g., ε-Fe_2C, ε'-$Fe_{2.2}C$, Fe_7C_3, θ-Fe_3C).[18] Many studies on active χ-Fe_5C_2 formation have been conducted by controlling the activation condition of inactive iron-oxides, and activation with CO gas has generally led to higher initial activity than that with synthesis gas or H_2.[19-23] In order to exclude the long extra activation step under CO or mixed gas, Yang et al. reported pure Hägg-carbide nanoparticles (around 20 nm), directly synthesized by the bromide-induced wet chemical method.[24] Besides adjusting an activation process, some additives, such as Cu, K, and Zn which affect the electronic and geometric properties of the catalyst surface were widely exploited to enhance CO conversion and product selectivity.[25-28] In particular, alkali metals have been considered excellent additives because they can easily donate electrons to active surfaces, enhancing the catalyst basicity.[29-30] For instance, the addition of potassium (K) into an iron catalyst as a base promoter has dramatically affected catalytic behavior, even in extremely small amounts (K/Fe at 0.01-0.04 atomic ratios).[31-33]

Recently, computational simulation based density functional theory (DFT) of surface reactions has become an effective tool for the design of new catalysts.[34-38] Along this line, several theoretical studies on iron carbide catalyst have involved using the computed activation energy, surface energy, and reaction energy.[39-41] In recent years, Sorescu reported the adsorption and dissociation of CO on K-doped Fe(100) surfaces and showed that an increase of the surface area covered by the K could lead to dramatically enhanced adsorption or dissociation behaviors.[42-43] Huo et al. explained the enhanced activity of the K-promoted metallic Fe catalyst theoretically and experimentally, and proposed that the main reason for enlarged active facets was the controlled Fe-crystal growth rate induced by added K.[44] However, the optimum atomic ratio of K per Fe, especially in the

χ-Fe_5C_2 structure for FTS, has not been clearly described in either theory or experiment, thus far.

Herein, we report a facile new method for synthesis of highly activated K-doped χ-Fe_5C_2/charcoal catalysts via melt-infiltration of the iron salt and subsequent incipient wetness impregnation of K precursors. The design was based on DFT calculation aimed at achieving the K addition effect. The obtained K-doped χ-Fe_5C_2/charcoal catalyst (K/Fe atomic ratio = 0.075) showed the highest activity (1.54×10^{-4} $mol_{CO}\bullet g_{Fe}^{-1}\bullet s^{-1}$), as well as good selectivity for gasoline-range (C_5-C_{12}) hydrocarbon products in the high-temperature FTS reaction under 320℃ and at 15 bar. The resulting activity of the optimally K-doped χ-Fe_5C_2/charcoal catalyst is comparable to the highest value previously reported among various supported-iron nanocatalysts.[16] In addition, this catalyst design based on DFT simulation and the simple synthesis method could remarkably reduce the optimization process by the conventional time-consuming trial-and-error method, for complicated catalysts with promoters.

2. Experimental Section

Chemicals: Iron nitrate nonahydrate ($Fe(NO_3)_3\bullet9H_2O$, ACS reagent, ≥ 98%), activated charcoal (~100 mesh particle size, powder), K_2CO_3 (powder, reagent grade, ≥ 98%), glass beads (425~600 μm size), and anhydrous ethanol were purchased from Aldrich. The chemicals were used as received without further purification.

Computations: DFT calculations were performed using the Vienna *ab initio* simulation package (VASP). This plane-wave code employs a projected, augmented wave with a generalized gradient approximation (PAW-GGA) for the exchange-correlation functional using the PBE method.[45] We performed geometric optimizations by minimizing the total energy of the unit cell using a conjugated-gradient algorithm to relax the ions. The Fe_5C_2 phase has a monoclinic structure and contains 20 Fe and 8 C atoms per unit cell. The corresponding optimized lattice parameters are in good agreement with the results of previous studies: a = 11.580 Å, b = 4.508 Å, c = 4.994 Å, and β = 97.64°.[46] For the Fe_5C_2 surface, we focused on the stable surface structure to estimate and characterize the reactivity of the Fe_5C_2 surfaces in the presence of K. The Fe_5C_2 (010) layer has an identical arrangement of atoms within the plane; however, every other plane is displaced laterally in the [100] direction by half the length of the unit cell, thereby generating a stacking sequence that repeats in the [010] direction every second layer. The Fe_5C_2 (010) surface termination exposes the repeating (010) plane. This surface is obtained by cleaving the conventional monoclinic unit cell of bulk Fe_5C_2 parallel to the (010) Miller plane at a fractional displacement of 0.25 along the unit-cell axis. The energy cutoff (400 eV) and a (5×5×1) Monkhorst–Pack grid were used for k-point sampling. The adsorption energy (E_{ad}) of the CO and K for each reaction was computed according to:

$$E_{ad} = E_{x/surface} - E_{surface} - E_x \quad (1)$$

where $E_{x/surface}$, E_x, and $E_{surface}$ are the total energies of the adsorbed system, the adsorbate (x = CO, K), and the clean surface, respectively. A negative adsorption energy corresponds to an energetically favorable adsorption site on the surface. Values that are more negative correspond to stronger adsorption. The electronic charge transfer on the atoms was computed using the Bader charge. The variation of electronic charge between the adsorbed and non-adsorbed states of a specific adsorbate was calculated according to:

$$\Delta q_x = q_{x(adsorbed)} - q_{x(non\text{-}adsorbed)} \quad (2)$$

where q_x represents the electronic charge of the adsorbate (x = CO, K). A negative Bader-charge value indicates that the electrons are transferred from the surface to the adsorbate. The dissociation energy barrier (E_b) for each reaction was computed according to:

$$E_b = E_{TS} - E_{IS} \quad (3)$$

where E_b, E_{TS}, and E_{IS} are the energy barrier of the elementary step, the total energy at the transition state, and the total energy at the initial state, respectively.

The reaction energy (ΔE) for each reaction was computed according to:

$$\Delta E = E_{FS} - E_{IS} \quad (4)$$

where E_{TS}, E_{FS}, and E_{IS} are the energy barrier for the elementary step, the total energy at the final state, and the total energy at the initial state, respectively. We employed the climbing image nudged elastic band (CI-NEB) method and constructed the minimum energy path (MEP).

Preparation of χ-Fe_5C_2/charcoal catalyst: To prepare a K-free χ-Fe_5C_2/charcoal catalyst, 1.85g of $Fe(NO_3)_3\bullet9H_2O$ was physically ground with 1.0 g of activated charcoal in a mortar for several minutes under ambient conditions until the powder was homogeneously black. Then, the mixed powders were placed in a polypropylene bottle and aged at 323 K in an oven. After aging for 24 h, the sample was cooled in ambient atmosphere and transferred to an alumina boat in a tube-type furnace. Finally, the iron-incorporated charcoal powder was slowly heated at a ramping rate of 2.7 °C/min up to 623K under a CO flow of 200 mL/min. The sample was allowed at 623 K for 4h under the continuous CO flow. After the thermal treatment, the resulting black powder was cooled down to room temperature, and then submerged into anhydrous ethanol (20 mL) under N_2 flow in order to prevent rapid surface oxidation. The χ-Fe_5C_2/charcoal powders were simply separated by magnetic force and completely dried in a vacuum oven at 323 K.

Synthesis of K-doped χ-Fe_5C_2/charcoal catalyst: For the syntheses of K-doped χ-Fe_5C_2/charcoal catalysts, stock solution with different concentrations of aqueous K_2CO_3 solution in distilled water were used (57.2 mM for K/Fe = 0.025, 114.6 mM for K/Fe = 0.05, 171.9 mM for K/Fe = 0.075, 229.2 mM for K/Fe = 0.1). The incipient wetness method was used to merge 1.0 mL of stock solution with the dried χ-Fe_5C_2/charcoal powder. Next, the K-incorporated sample was transferred to an alumina boat in a tube-type furnace, and then slowly heated at a ramping rate of 2.7 °C/min to 623 K under a CO flow of 200 mL/min. After the thermal treatment, the resulting black powder was cooled to room temperature, and then were submerged into anhydrous ethanol (20 mL) under N_2 flow. Finally, the K-doped χ-Fe_5C_2/charcoal powder was separated and dried in a vacuum oven at 323 K.

Catalytic test: The Fischer-Tropsch synthesis reaction was carried out in a fixed-bed reactor composed of stainless steel (5 mm inner diameter and 180 mm length). The catalyst (0.3g) was diluted with glass beads (3.4g) to prevent hot spot generation due to a serious exothermic reaction of catalysts and then placed in the fixed-bed reactor. The catalyst was reactivated under a CO flow of 40 mL/min at 623 K for 4 h. After the activation treatment, the reaction was performed at 320℃ and 15 bar using synthesis gas (H_2/CO = 1.0, GHSV=8.0 NL•g_{cat}^{-1}•h^{-1}). The composition of the outlet gases was analyzed using an online gas chromatograph (Agilent, 3000A Micro-GC) equipped with molecular sieve and plot Q columns. The gas flow rates were measured using a wet-gas flow meter (Shinagawa Corp.). After catalytic reaction, the mixtures of liquid hydrocarbon products and water were isolated in the cold trap at 1℃, and solid hydrocarbons were obtained in the hot trap at 240 ℃. The isolated wax and liquid products were analyzed by an offline gas chromatograph (Agilent, 6890 N) with a simulated distillation method (ASTM D2887).

Characterization: The obtained iron carbide/charcoal catalysts were characterized by TEM (Omega EM912 operated at 120 kV, Korea Basic Science Institute), HRTEM (Tecnai G2 F30 operated at 300 kV, KAIST), and an EDX (attached to a F30 Tecnai). For scanning TEM analysis, samples were prepared by putting a few drops of the corresponding colloidal solutions on lacey carbon coated copper grids (Ted Pellar, Inc). High power powder-XRD (Rigaku D/MAX-2500, 18kW) was also used for analysis. X-ray photoelectron spectroscopy (XPS) studies were carried out using a Sigma Probe (Thermo VG Scientific, Inc.) with a micro-focused monochromator X-Ray source. The samples for XPS were prepared by placing a few drops of the colloidal solutions on small pieces (5 mm × 5 mm) of gold wafer and then were allowed to dry under N_2 flow. Mössbauer spectra were obtained with a fixed absorber and a moving source. A Mössbauer spectrometer of the electromechanical type, with a 50 mCi ^{57}Co source in a rhodium matrix, was used in constant-acceleration mode. The Fe X-ray absorption spectra (XAS) were measured on Beam-line 1D of the Pohang Accelerator Laboratory (PAL). N_2 sorption isotherms were measured at 77 K with a TriStar II 3020 surface area analyzer. Before measurement, the samples were degassed in a vacuum at 300℃ for 4 h.

3. Results and Discussion

3.1. DFT Calculation for K-doped Fe_5C_2 surfaces

Prior to the catalyst preparation, we modeled a super-cell surface with a slab of five iron layers and three carbon layers. The surface with the "hexagonal" and "square" iron-atom formations was exposed. The K and CO adsorption onto the Fe_5C_2 (010) surface, which consists of a 4-fold hollow, 3-fold hollow, bridge, and top site, were simulated (Supporting Information, Figure S1). The first K adsorption, at the K/Fe atomic ratio = 0.025, was simulated by the clean and Fe-terminated surface of Fe_5C_2 (010) containing 40 Fe and 16 C atoms for several adsorption sites (Figure 1a). Among the possible adsorption sites, the K atom preferentially adsorbs on the 3-fold hollow site of Fe because it has the strongest adsorption energy -2.48 eV (Supporting Information, Table S1). The Bader charge (q_K) at K/Fe = 0.025

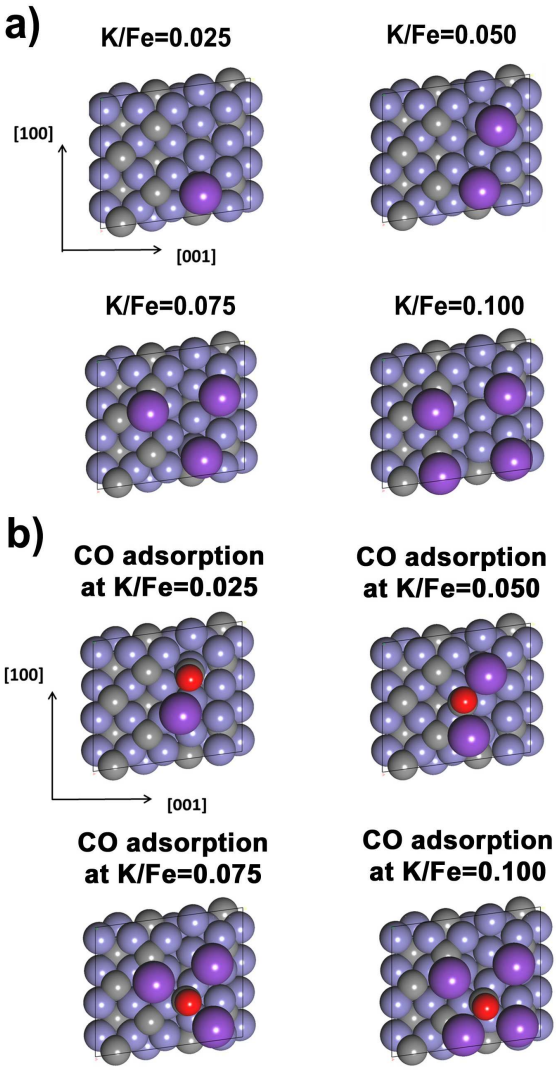

Fig. 1 Surface configurations of (a) stable K adsorption on a clean χ-Fe_5C_2 surface, and (b) stable CO adsorption on a K-doped Fe_5C_2 surface with a controlled K/Fe ratio. The black, blue, red, and violet balls represent carbon, iron, oxygen, and potassium atoms, respectively.

was 0.86, which resulted from the electron-charge transfers to the catalyst surface from K. Afterward, another K atom adsorbs onto the nearest stable site, and this process is repeated. All Bader charges for K on the Fe- and C-terminated sites indicated positive values because K donates electrons to catalyst surface in the role of a Lewis base. The CO adsorption and dissociation properties, after K-doping of the surface, were also affected nearby K atoms (Figure 1b). From the calculations of these models, the adsorption energies of CO molecules on the K-doped χ-Fe_5C_2 surfaces were obtained (Table 1). As more K atoms spread over the χ-Fe_5C_2 surface, the CO adsorption energy and C-O bond distance (d_{C-O}) increases. Strong CO adsorption was observed simultaneous with increased C-O bond length. The CO adsorption energies of the K-doped χ-Fe_5C_2 surfaces showed -2.26 eV at K/Fe = 0.025, -2.41 eV at K/Fe = 0.050, -2.52 eV at K/Fe = 0.075, and -2.64 eV at K/Fe = 0.100, respectively, indicating the significant K effect on CO adsorption. All Bader

charges for CO showed negative values due to the charge transferred from the catalyst surface to CO molecules. Unexpectedly, the energy barrier for CO dissociation and reaction energy at the K/Fe ratio = 0.075 was lower than those for K/Fe = 0.100, calculated to be 1.40 eV and -1.28 eV, respectively.

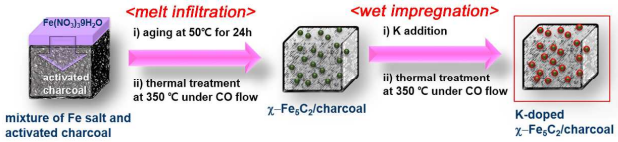

Scheme 1. Stepwise synthetic scheme of an highly activated K-doped χ-Fe_5C_2/charcoal catalyst.

Table 1. Calculated adsorption energies (E_{ad}), distances for CO, and energy barriers (E_b) and reaction energies (ΔE) for CO dissociation on Fe_5C_2 surfaces.

K:Fe atomic ratio	E_{ad}(eV) of CO	dc-o (Å)	q_{co}(Δe)	E_b (eV) for CO dissociation	Δ E(eV)
K-free	-2.08	1.211	-0.86	1.74	-1.12
K/Fe=0.025	-2.26	1.224	-0.96	1.64	-1.16
K/Fe=0.050	-2.41	1.248	-1.09	1.53	-1.21
K/Fe=0.075	-2.52	1.262	-1.19	1.40	-1.28
K/Fe=0.100	-2.64	1.275	-1.38	1.48	-1.22

3.2. Synthesis of K-doped χ-Fe_5C_2/charcoal catalyst

To evaluate the obtained calculation data, we introduced new model catalysts through a melt-infiltration process and an incipient wetness method controlling the K/Fe atomic ratios (Scheme 1). First, active iron carbide nanoparticles embedded in a porous charcoal support were successfully obtained via two simple steps: an aging step and a thermal decomposition step. In the first step, an $Fe(NO_3)_3$•$9H_2O$ salt was homogeneously mixed with activated charcoal by grinding at room temperature. This mixture was subsequently melt-infiltrated into mesoporous charcoal by aging at 323 K for 24 h in an oven. This melt-infiltration process, which is also well known as the solvent-free method or solid-liquid route, has already been employed for preparation of some supported catalysts due to its remarkable convenience and speed.[47-48] In the second step, the melt-infiltrated Fe salt was transformed to active iron carbide nanoparticles by thermal decomposition at 623 K under a flow of CO.

The transmission electron microscopy (TEM) image shows the incorporated iron carbide nanoparticles with an average diameter of 17.8±2.8 nm (Figure 2a and 2i). In the high-resolution TEM (HRTEM) image, the iron carbide particle in the porous charcoal shows its single crystalline nature and the lattice distance was measured to be 0.205 nm, consistent with the value of the Fe_5C_2 (510) plane (Figure 2b). Next, K-doped Fe_5C_2 particles were obtained by impregnating the K_2CO_3 salt as a K source into the Fe_5C_2/charcoal powders and thermally treating them. The K/Fe ratios in the K-doped Fe_5C_2 particles were controlled using

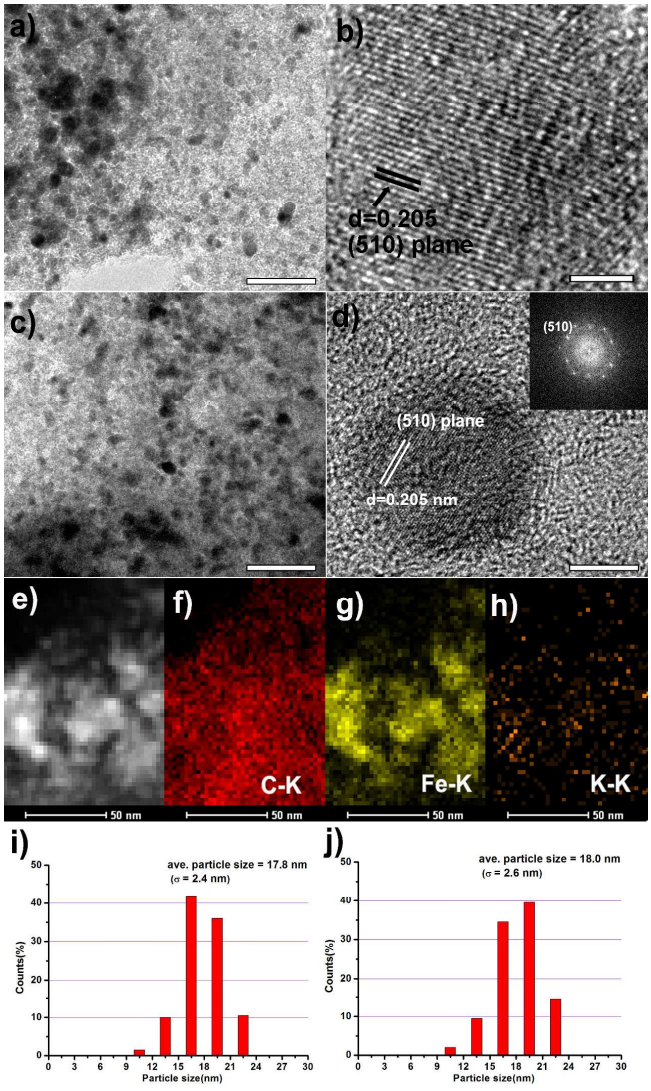

Fig. 2 TEM images of (a) K-free and (c) K-doped χ-Fe_5C_2 (K/Fe=0.075) nanoparticles on activated charcoal, and HRTEM images of (b) K-free and (d) K-doped χ-Fe_5C_2 single particle with corresponding FT pattern (inset of d). (e) HADDF-STEM image and (f-h) elemental mapping for the K-doped χ-Fe_5C_2/charcoal catalyst (K/Fe = 0.075). Particle size distribution histograms of (i) K-free and (j) K-doped χ-Fe_5C_2 nanoparticles (K/Fe=0.075). The bars represent 100 nm (a,c), 2 nm (b), and 5 nm (d), respectively.

different concentrations of aqueous K_2CO_3 solution. The K-doped Fe_5C_2 nanoparticles at the K/Fe ratio = 0.075 were well dispersed in the charcoal with its relatively narrow size distribution (18.0±2.6 nm), remaining without any significant particle agglomerations even after high-temperature thermal retreatment of the Fe_5C_2 particles at 623 K (Figure 2c and 2j). The HRTEM image and corresponding Fourier-transform (FT) pattern show that the final K-doped Fe_5C_2 particle with a spherical shape was a single crystal with the distance of 0.205 nm between neighboring fringes (Figure 2d). High angle annular dark field-scanning transmission electron microscopy (HAADF-STEM) and elemental mapping of carbon (red), iron (green), and potassium (brown) clearly showed the uniform distribution of each component (Figure 2e-h). While carbon could be detected over

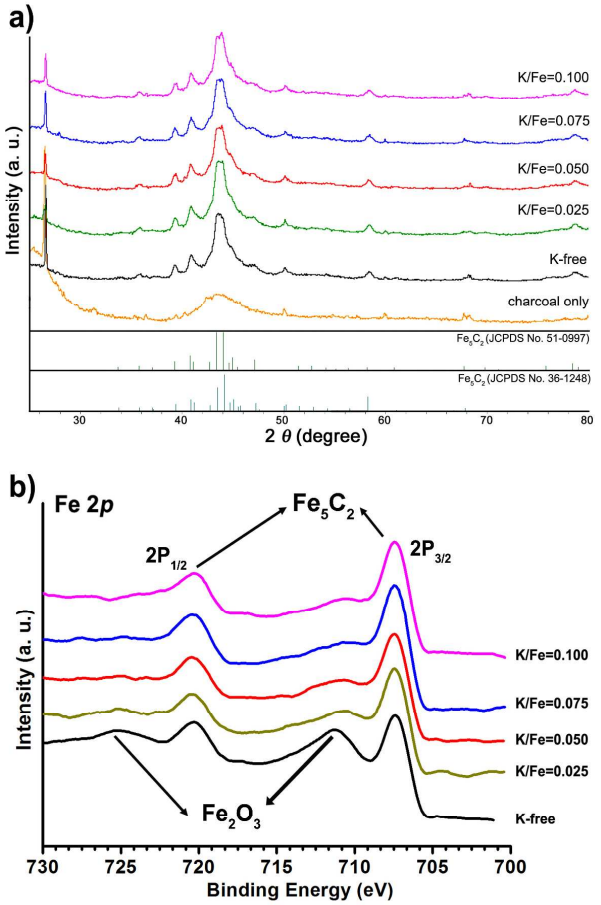

Fig. 3 (a) XRD and (b) XPS spectra of K-free and K-doped χ-Fe_5C_2 nanoparticles on activated charcoal.

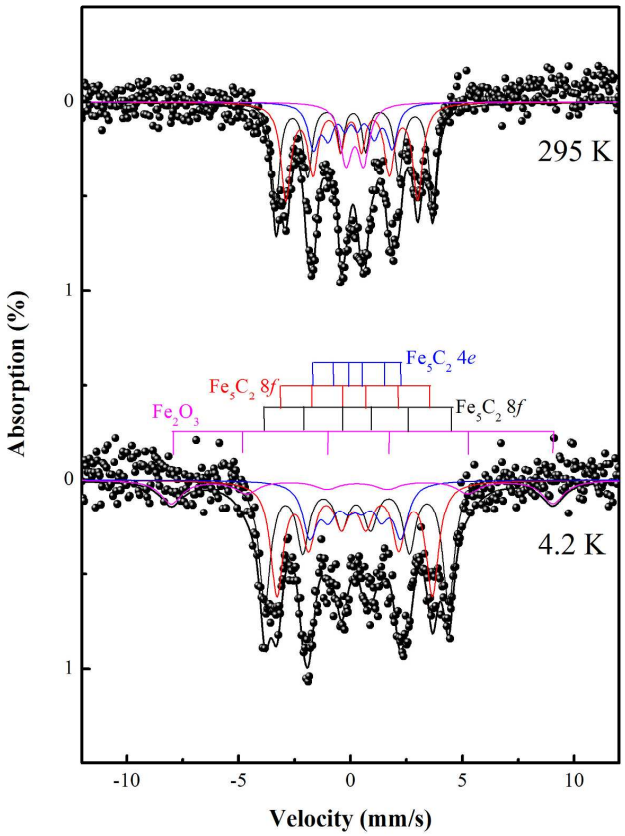

Fig. 4 Mössbauer spectra of K-free χ-Fe_5C_2 nanoparticles on activated charcoal at 4.2 and 295 K.

the whole area, potassium was mainly found in the Fe-rich area, meaning that the added potassium atoms were well adsorbed onto the Fe_5C_2 particles in charcoal. All the K-doped Fe_5C_2 particles even with different K/Fe ratios showed similar average particle sizes, measured to be 17.8±2.7 nm at K/Fe = 0.025, 18.2±2.8 nm at K/Fe = 0.050, and 20.4±3.9 nm at K/Fe = 0.100 (Figure S2). In Figure 3a, the X-ray diffraction (XRD) spectra show that all iron carbide particles are well-matched with the two Hägg-carbide phases (JCPDS No. 36-1248 and No. 51-0997; space group, C2/c). No significant differences in the XRD spectra for all samples were observed. A sharp peak at 2θ = 26.5° corresponded to a crystalline carbon structure in the activated charcoal (JCPDS No. 26-1077). The crystallite sizes of K-free and K-doped Fe_5C_2 estimated from the FWHM of the (020) diffraction peaks were 20.0 nm at K-free, 20.8 nm at K/Fe = 0.025, 20.8 nm at K/Fe = 0.050, 19.9 nm at K/Fe = 0.075, and 21.0 nm at K/Fe = 0.100. The calculated single crystallite sizes were very close to the average particle sizes measured in the TEM images, demonstrating the single crystal nature. To investigate the surface states in the K-free and K-doped Fe_5C_2 particles, the core-level X-ray photoelectron spectroscopy (XPS) spectrum of Fe for each sample was measured (Figure 3b). All XPS spectra show two sets of peaks from iron carbide and iron oxide in the range of Fe $2p_{3/2}$ and $2p_{1/2}$ orbital signals. In the spectra, the surfaces of the Fe_5C_2 nanoparticles, for both the K-free and K-doped samples, were observed as partially-oxidized forms. Even though the fresh catalyst powders were passivated by ethanol, the slight surface oxidation of the highly active Fe_5C_2 nanoparticles was inevitable due to atmospheric exposure during the sampling processes. Interestingly, all K-doped Fe_5C_2 nanoparticles showed much better stability against oxidation than did K-free Fe_5C_2 nanoparticles, because the neighbor K could be more easily oxidized than Fe_5C_2. Mössbauer investigation has been applied to measure the rate of carbiding of iron during FTS reaction, over a supported iron catalyst.[49-50] The specific portion of the pure Hägg-carbide species in several iron carbide phases could be ascertained by Mössbauer spectroscopy. To investigate the distribution of the iron based emergent materials and hyperfine interaction, the Mössbauer spectra of the K-free Fe_5C_2/charcoal were obtained at 4.2 and 295 K. The Mössbauer spectra show the superposition of three-sextets for Fe sites, corresponding to only χ-Fe_5C_2 crystallography sites. Other iron carbide phases, such as $Fe_{2.2}C$, Fe_7C_3, Fe_3C, were not observed. The one-doublet at 295 K is analyzed to be a Fe_2O_3 phase (Figure 4). The relative areas of χ-Fe_5C_2 and Fe_2O_3, which were obtained from the fitted Mössbauer parameters, were calculated to be 88% and 12%, respectively (Table S2).

To check the oxidation state in the bulk form and binding environment for Fe atoms within C molecules for the K-doped χ-Fe_5C_2/charcoal, X-ray absorption spectroscopy (XAS) measurement was conducted. This is based on electron excitation

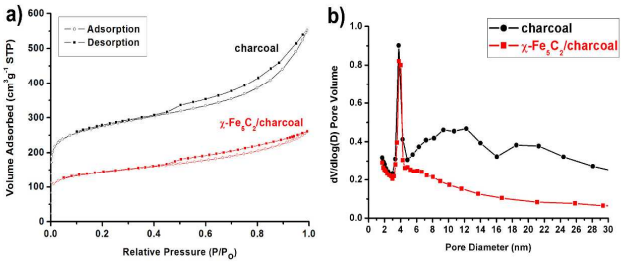

Fig. 5 (a) N_2 adsorption/desorption isotherms of initial charcoal and K-doped χ-Fe_5C_2 on activated charcoal (K/Fe=0.075), (b) Pore size distribution diagrams of K-doped χ-Fe_5C_2 on activated charcoal (K/Fe=0.075) calculated from desorption branches using the BJH method.

by an X-ray beam which moves an electron from a core orbital to an unoccupied molecular orbital. In the X-ray absorption, near-edge structure (XANES) region from an absorption edge to 7162 eV, Fe pre-edge peaks for all K-doped χ-Fe_5C_2/charcoal were observed at 7112eV, which corresponds with that of metallic Fe (Figure S3a-b). All the extended X-ray absorption fine structure (EXAFS) patterns for K-doped χ-Fe_5C_2/charcoal showed two major peaks of the first two coordination shells of Fe_5C_2, originating from Fe-C (~1.6Å) and Fe-Fe (~2.2Å) scattering (Figure S3c-d).

The pore volume and size of the porous charcoal support were crucial to determine the loading ratio of iron salt by the melt-infiltration method. N_2 sorption experiments at 77 K for the K-doped χ-Fe_5C_2/charcoal catalyst at K/Fe = 0.075 exhibited type IV adsorption-desorption hysteresis with delayed capillary evaporation at a relative pressure of 0.5 (Figure 5a). The Brunauer-Emmett-Teller (BET) surface areas of the initial charcoal and the K-doped χ-Fe_5C_2/charcoal were calculated to be 1010 $m^2 \cdot g^{-1}$ and 525 $m^2 \cdot g^{-1}$, respectively. The total pore volumes were also measured to be 0.85 $cm^3 \cdot g^{-1}$ for the initial charcoal and 0.40 $cm^3 \cdot g^{-1}$ for the K-doped χ-Fe_5C_2/charcoal. The small pore sizes of the initial charcoal and K-doped χ-Fe_5C_2/charcoal were found to be equal (3.8 nm) using the Barrett-Joyner-Halenda (BJH) method from their desorption branches (Figure 5b).

High Fe-loading with uniform particle dispersion in the supported Fe catalyst is also very important. The Fe-loading content for the K-free and K-doped catalysts was calculated to be approximately 20 wt% on the basis of Fe converted from the iron nitrate salt after thermal treatment.

3.3. High-temperature Fischer-Tropsch Synthesis reaction

High-temperature FTS reaction tests were carried out at 15 bar, 320℃, and an H_2/CO ratio of 1 using the model catalysts. The catalytic activity was noted as iron-time-yield (FTY, i.e., the number of CO moles converted to hydrocarbons per gram of iron per second) over time-on-stream (TOS). These FTY values reflect the CO conversion and hydrocarbon selectivity of each FTS catalyst. As expected from the calculation results, the K-doped catalysts showed much better catalytic performance, with higher FTY values, than that of the K-free catalyst (Figure 6). In addition, the initial activity during 48 h in all K-doped Fe_5C_2/charcoal catalysts was superior to that of the K-free catalyst, demonstrating their high and fast activation with K. The relatively long induction period during FTS over the K-free catalyst is mainly due to more difficult phase transformation from

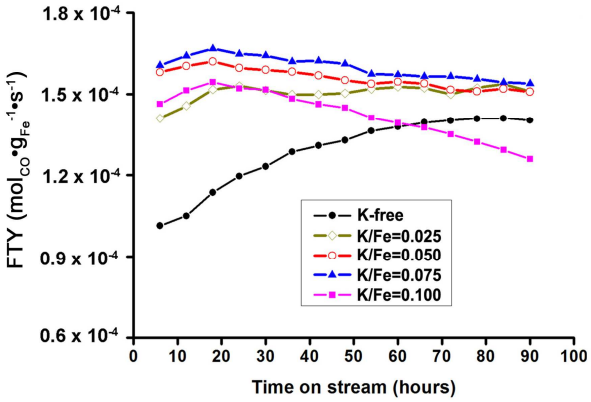

Fig. 6 Catalytic performance of K-free and K-doped χ-Fe_5C_2/charcoal catalysts for high-temperature FTS. The reaction tests were conducted at 320 ℃ and at 15 bar and a H_2:CO ratio of 1. FTY represents the number of CO moles converted to hydrocarbons per gram of iron per second.

the partially oxidized iron to activated Fe_5C_2 species. In particular, the K-doped catalyst at K/Fe = 0.075 showed a very high CO conversion (>95%) with good C_{5+} selectivity (~50%) (Figures S4d and S5d). Moreover, the selectivity for methane as a side product was also very low (~5%), comparable to 12% of the K-free catalyst (Figures S5). Based on these results, at K/Fe = 0.075, the highest activity (1.54×10^{-4} $mol_{CO} \cdot g_{Fe}^{-1} \cdot s^{-1}$) was obtained for up to 90 h. This FTY value is much higher than those of the previously reported highest value (8.48×10^{-5} $mol_{CO} \cdot g_{Fe}^{-1} \cdot s^{-1}$) in various supported iron nanostructures.[16] In the previous works, K-dope Fe on carbon spheres and K-doped Fe on carbon nanotubes showed relatively low activities of 1.8×10^{-5} $mol_{CO} \cdot g_{Fe}^{-1} \cdot s^{-1}$ and 2.8×10^{-5} $mol_{CO} \cdot g_{Fe}^{-1} \cdot s^{-1}$.[11,15] We believe that the enhanced activity mainly originates from the electrostatic interaction by the added K,[51-52] not from any changes of active facets, because significant differences among the catalyst surface structures and crystallite sizes were not detected in the XRD data. On the other hand, the activity at K/Fe = 0.1 gradually decreased to 1.26×10^{-4} $mol_{CO} \cdot g_{Fe}^{-1} \cdot s^{-1}$ under the same reaction conditions. At K/Fe = 0.1, the deactivation with low FTY values after 20 h is closely linked to increased CO_2 selectivity and decreased C_{5+} selectivity (Figure S5e). As seen in the DFT calculation results of Table 1, the catalyst at K/Fe = 0.1 showed unfavorable reaction energy (-1.22 eV) for CO dissociation than -1.28 eV of K/Fe = 0.075, even though it had the strongest CO adsorption energy (-2.64 eV). Because of the steric effect of CO caused by a large amount of neighboring K, the CO dissociation energy barrier (1.48 eV) at K/Fe = 0.1 was higher than 1.40 eV at K/Fe = 0.075.

The total hydrocarbon (HC) product yields (gram of generated hydrocarbons per gram of iron per second) for the K-free and K-doped χ-Fe_5C_2 catalysts were measured after 90 h on stream of reaction, calculated by the sum of specific product yields (Figure 7, Table 2). The specific product yield for each sample was obtained by gas chromatography (GC) analysis of gaseous products (C_1-C_4) and simulated distillation (SIMDIS) analysis of isolated solid (wax) and liquid (oil) products. In all K-doped Fe_5C_2 catalysts, total HC product yields higher than that of the K-free χ-Fe_5C_2 catalyst were obtained. Among the K-doped χ-Fe_5C_2 catalysts, the total HC product yield at K/Fe = 0.075 was the best, calculated to be 1.41×10^{-3} $g_{HC} \cdot g_{Fe}^{-1} \cdot s^{-1}$. In contrast, the K-free

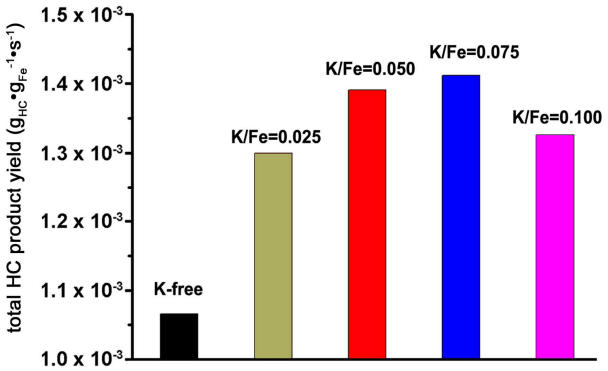

Fig. 7 Total hydrocarbon product yield for K-free and K-doped χ-Fe_5C_2/charcoal catalysts after 90 h on stream.

Table 2 Specific product yields for K-free and K-doped χ-Fe_5C_2/charcoal catalysts after 90 h on stream

Cat.	Specific product yield ($10^{-4}g_{HC}$•g_{Fe}^{-1}•s^{-1})					
	CH_4	C_2-C_4 olefins	C_2-C_4 parafins	C_5-C_{12}	C_{13}-C_{18}	C_{19+}
K-free	4.11	1.08	4.67	0.57	0.15	0.09
K/Fe =0.025	3.10	2.05	3.47	3.63	0.53	0.26
K/Fe =0.050	1.60	3.44	1.24	4.80	1.44	1.38
K/Fe =0.075	1.50	3.36	1.10	4.86	1.64	1.67
K/Fe =0.100	1.20	3.07	0.66	4.50	1.73	2.11

catalyst showed very low total HC productivity (1.07×10^{-3} g_{HC}•g_{Fe}^{-1}•s^{-1}). In the specific product yields, the K-addition effect was observed to be dramatic. In all the K-doped χ-Fe_5C_2 catalysts, the methane product was significantly decreased compared to that of K-free χ-Fe_5C_2. In particular, regarding the production of gasoline range products (C_5-C_{12}), the K-doped χ-Fe_5C_2 catalyst at K/Fe = 0.075 showed a 4.86×10^{-4} g_{HC}•g_{Fe}^{-1}•s^{-1} product yield, which was 8.5 times higher than that of the K-free χ-Fe_5C_2 catalyst. For the product analysis, the hydrocarbon distributions were also measured after 90 h (Table S3). The distributions for lower olefins and gasoline at K/Fe = 0.075 were ~24wt% and ~34wt% in the total hydrocarbon products, respectively.

4. Conclusions

We have conducted theoretical and experimental research on K-free and K-doped χ-Fe_5C_2 on charcoal nanocatalysts. The DFT calculation of the K doping effects on the active Hägg-carbide phase suggested that the optimum K-doping ratio is K/Fe = 0.075, consistent with the experiment results. The K-doped χ-Fe_5C_2/charcoal nanocatalysts with a controlled K/Fe atomic ratio, were prepared via a facile melt-infiltration process and incipient wetness method, showed the highest FTY values with the best total HC product yield in high-temperature FTS under 320℃ and at 15 bar. It is anticipated that this approach based on computational simulation will be useful in creating more delicate and rational designs of heterogeneous catalysts by improving our understanding of some additive effects.

Acknowledgements

This work was conducted under the framework of the Research and Development Program of the Korea Institute of Energy Research (KIER) (B4-2432-03). The authors greatly appreciate the technical support of Mr. Seong Bum Yoo (Hanbat National University, Republic of Korea).

Notes and references

[a] *Clean Fuel Laboratory, Korea Institute of Energy Research, 152 Gajeong-Ro, Daejeon, 305-343, Korea. Tel: 82-42-860-3663; E-mail: jungh@kier.re.kr*
[b] *Department of Materials Science and Engineering, Korea Advanced Institute of Science and Technology, Daejeon, 305-701, Korea.*
[c] *Department of Physics, Kookmin University, Seoul, 136-702, Korea.*

† Electronic Supplementary Information (ESI) available: Hägg-carbide model of a 1x2 super-cell, TEM images and particle size distribution histograms of K-doped χ-Fe_5C_2 nanoparticles, Fe K-edge X-ray absorption spectra, and CO conversion and selectivity data for K-free and K-doped χ-Fe_5C_2/charcoal catalysts. See DOI: 10.1039/b000000x/

1 Q. Zhang, J. Kang, Y. Wang, *ChemCatChem.*, 2010, **2**, 1030.
2 R. Lique, A. R. Campelo, J. M. Campelo, A. A. Romero, J. L. Valverde, P. Sanchez, Energy Environ. Sci., 2012, **5**, 5186.
3 M. E. Dry, *Catal. Today*, 2002, **71**, 227.
4 A. P. Steynberg, M. E. Dry, Eds. Studies in Surface Science and Catalysis: Fischer-Tropsch Technology; Elsevier: Amsterdam, 2004; Vol. **152**.
5 A. de Klerk, *Energy Environ. Sci.*, 2011, **4**, 1177.
6 A. de Klerk, *Green Chem.*, 2007, **9**, 560.
7 A. P. Steynberg, R. L. Espinoza, B. Jager, A. C. Vosloo, *Appl. Catal. A: Gen.*, 1999, **186**, 41.
8 H.-J. Wan, B.-S. Wu, C.-H. Zhang, H.-W. Xiang, Y.-W. Li, B.-F. Xu, F. Yi, *Catal. Commun.*, 2007, **8**, 1538.
9 C.-H. Zhang, H.-J. Wang, Y. Yang, H.-W. Xiang, Y.-W. Li, *Catal. Commun.*, 2006, **7**, 733.
10 J. Shen, B. Guang, M. Tu, Y. Chen, *Catal. Today*, 1996, **30**, 77.
11 H. Xiong, M. Moyo, M. A. M. Motchelaho, L. L. Jewell, N. Coville, *J. Appl. Catal. A.: Gen.*, 2010, **388**, 168.
12 R. M. Abbaslou, A. Tavassoli, J. Soltan, A. K. Dalai, *Appl. Catal. A.: Gen.*, 2009, **367**, 47.
13 J. F. Bengoa, A. M. Alvarez, M. V. Cagnoli, N. G. Gallegos, S. G. Marchetti, *Appl. Catal. A.: Gen.*, 2007, **325**, 68.
14 G. Yu, B. Sun, Y. Pei, S. Xie, S. Yan, M. Qiao, K. Fan, X. Zhang, B. Zong, *J. Am. Chem. Soc.*, 2010, **132**, 935.
15 J. Lu, L. Yang, B. Xu, Q. Wu, D. Zhang, S. Yuan, Y. Zhai, X. Wang, Y. Fan, Z. Hu, *ACS Catal.*, 2014, **4**, 613.
16 H. M. T. Galvis, J. H. Bitter, C. B. Khare, M. Ruitenbeek, A. I. Dugulan, K. P. de Jong, *Science*, 2012, **335**, 835.
17 H. M. T. Galvis, J. H. Bitter, T. Davidian, M. Ruitenbeek, A. I. Dugulan, K. P. de Jong, *J. Am. Chem. Soc.*, 2012, **134**, 16207.
18 E. de Smit, B. M. Weckhuysen, *Chem. Soc. Rev.*, 2008, **37**, 2758.
19 D. B. Bukur, K. Okabe, M. P. Rosynek, C. Li, D. Wang, K. R. P. M. Rao, G. P. Huffman, *J. Catal.*, 1995, **155**, 353.
20 A. Sarkar, D. Seth, A. K. Dozier, J. K. Neathery, H. H. Hamdeh, B. H. Davis, *Catal. Lett.*, 2007, **117**, 1.
21 E. de Smit, M. M. van Schooneveld, F. Cinquini, H. Bluhm, P. Sautet, F. M. F. de Groot, B. M. Weckhuysen, *Angew. Chem. Int. Ed.*, 2011, **50**, 1584.
22 T. Herranz, S. Rojas, F. J. Pérez-Alonso, M. Ojeda, P. Terreos, J. L. Fierro, *J. Catal.*, 2006, **243**, 199-211.
23 E. de Smit. F. Cinquini, A. M. Beale, O. V. Safonova, W. van Beek, P. Sautet, B. M. Weckhuysen, *J. Am. Chem. Soc.*, 2010, **132**, 14928.

24 C. Yang, H. Zhao, Y. Hou, D. Ma, *J. Am. Chem. Soc.*, 2012, **134**, 15814.
25 R. J. O'Brien, L. Xu, D. R. Milburn, Y.-X. Li, K. J. Klabunde, B. H. Davis, *Top. Catal.*, 1995, **2**, 1.
26 G. Zhao, C. Zhang, S. Qin, H. Xiang, Y. Li, *J. Mol. Catal. A: Chem.*, 2008, **286**, 137.
27 S. Li, S. Krishnamoorthy, A. Li, G. D. Meitzner, E. Iglesia, *J. Catal.*, 2002, **206**, 202.
28 N. Lohitharn, J. G. Goodwin Jr., E. Lotero, *J. Catal.* 2008, **255**, 104.
29 A. N. Pour, M. R. Housaindokht, S. F. Tayyari, J. Zarkesh, M. R. Alaei, *J. Nat. Gas Sci. Eng.*, 2010, **2**, 61.
30 W. Ngantsoue-Hoc, Y. Zhang, R. J. O'Brien, M. Luo, B. H. Davis, *Appl. Catal. A: Gen.*, 2002, **236**, 77.
31 S. Li, A. Li, S. Krishnamoorthy, E. Iglesia, *Catal. Lett.,* 2001, **4**, 197.
32 B. Graf, M. Muhler, *Phys. Chem. Chem. Phys.*, 2011, **13**, 3701.
33 Y. Yang, H.-X. Xiang, Y.-Y. Xu, L. Bai, Y.-W. Li, *Appl. Catal. A: Gen*. 2004, **266**, 181.
34 C. Harding, V. Habibpour, S. Kunz, A. N.-S. Farnbacher, U. Heiz, B. Yoon, U. Landman, *J. Am. Chem. Soc.*, 2009, **131**, 538.
35 J. K. Nørskov, T. Bligaard, J. Rossmeisl, C. H. Christensen, *Nature Chem.,* 2009, **1**, 37.
36 X.-Q. Zhang, E. Iype, S. V. Nedea, A. P. J. Jansen, B. M. Szyja, E. J. M. Hensen, R. A. van Santen, *J. Phys. Chem. C*, 2014, **118**, 6822.
37 K. Honkala, A. Hellman, I. N. Remediakis, A. Logadottir, A. Carlsson, S. Dahl, C. H. Christensen, J. K. Nørskov, *Science*, 2005, **307**, 555.
38 F. Studt, F. Abild-Pedersen, T. Bligaard, R. Z. Sørensen, C. H. Christensem, J. K. Nørskov, *Science*, 2008, **320**, 1320.
39 D.-B. Cao, Y.-W. Li, J. Wang, H. Jiao, *J. Mol. Cat. A: Chem.*, 2011, **346**, 55.
40 S. Zhao, X.-W. Liu, C.-F. Huo, Y.-W. Li, J. Wang, H. Jiao, *J. Catal.* 2012, **294**, 47.
41 C.-F. Huo, Y.-W. Li, J. Wang, H. Jiao, *J. Am. Chem. Soc.,* 2009, **131**, 14713.
42 D. C. Sorescu, *Sur. Sci.*, 2011, **605**, 401.
43 D. C. Sorescu, *J. Phys. Chem. C.*, 2009, **113**, 9256.
44 C.-F. Huo, B.-S. Wu, P. Gao, Y. Yang, Y.-W. Li, H. Jiao, *Angew. Chem. Int. Ed.*, 2011, **50**, 7403.
45 G. Kresse, D. Joubert, *Phys. Rev. B*, 1999, **59**, 1758.
46 M. A. Petersen, J.-A. van den Berg, W. J. van Rensburg, *J. Phys. Chem. C,* 2010, **114**, 7863.
47 P. E. de Jongh, R. W. P. Wagemans, T. M. Eggenhuisen, B. S. Dauvillier, P. B. Radstake, J. D. Meeldijk, J. W. Geus, K. P. de Jong, *Chem. Mater.,* 2007, **19**, 6052.
48 T. M. Eggenhuisen, J. P. den Breejen, D. Verdoes, P. E. de Jongh, K. P. de Jong, *J. Am. Chem. Soc.,* 2010, **132**, 18318.
49 G. B. Raupp, W. N. Delgass, *J. Catal.*, 1979, **58**, 361.
50 J. W. Niemantsverdriet, A. M. Van der Kraan, W. L. Van Dijk, H. S. Van der Baan, *J. Phys. Chem.*, 1980, **84**, 3363.
51 Z.-P. Liu, P. Hu, *J. Am. Chem. Soc.*, 2001, **123**, 12596.
52 R. W. Gurney, *Phys. Rev.*, 1935, **47**, 479.

Cite this: DOI: 10.1039/c0xx00000x

www.rsc.org/xxxxxx

Full Papers

Graphical Abstract

The highly activated K-doped Hägg-carbide/charcoal nanocatalysts designed on the basis of DFT calculation were simply prepared through a melt-infiltration process and thermal activation at 623 K. The K-doped χ-Fe_5C_2/charcoal nanostructure at K/Fe=0.075 that bear small iron carbide particles of ~18 nm showed the highest FTY value and the best hydrocarbon yield as well as a good gasoline selectivity for high-temperature Fischer-Trospch reaction.